

# Insights into the function of silver as an oxidation catalyst by ab initio, atomistic thermodynamics

Wei-Xue Li,<sup>1</sup> Catherine Stampfl,<sup>1,2</sup> and Matthias Scheffler<sup>1</sup>

<sup>1</sup>*Fritz-Haber-Institut der Max-Planck-Gesellschaft,  
Faradayweg 4-6, D-14195 Berlin-Dahlem, Germany*

<sup>2</sup>*School of Physics, The University of Sydney, Sydney 2006 Australia*

(Dated: Received 24 April 2003)

To help understand the high activity of silver as an oxidation catalyst, e.g., for the oxidation of ethylene to epoxide and the dehydrogenation of methanol to formaldehyde, the interaction and stability of many different oxygen species at the Ag(111) surface has been studied for a wide range of coverages. Through calculation of the free energy, as obtained from density-functional theory and taking into account the temperature and pressure via the oxygen chemical potential, we obtain the phase diagram of O/Ag(111). Our results reveal that a *thin* surface-oxide structure is most stable for the temperature and pressure range of ethylene epoxidation and we propose it (and possibly other similar structures) contains the species actuating the catalysis. For higher temperatures, low coverages of chemisorbed oxygen are most stable, which could also play a role in oxidation reactions. For temperatures greater than about 775 K there are *no* stable oxygen species, except for the possibility of O atoms adsorbed at under-coordinated surface sites (i.e., imperfections, defects). At low temperatures ( $\lesssim 400$  K at atmospheric pressure), provided kinetic limitations can be overcome, thicker oxide-like structures are predicted. Due to their low thermal stability, however, they can be ruled out as playing an important role in the heterogeneous reactions under technical conditions. Bulk dissolved oxygen and a molecular ozone-like species adsorbed at a surface vacancy, as have been proposed in the literature, are found to be energetically unfavorable. The employed theoretical approach for calculating *free energies* and predicting the lowest energy structures in contact with species in the environment (“*ab initio*, atomistic thermodynamics”), affords investigation of a system that seamlessly connects standard ( $T = 0$  K) DFT results, characteristic of “typical” theoretical surface science studies, through to those valid for the conditions of catalysis. Though the error bar of the noted theoretical temperatures is noticeable ( $\pm \approx 55$  K), the identified trends and physical descriptions are useful.

PACS numbers: PACS: 82.65.Mq, 68.35.Md, 68.43.Bc

## I. INTRODUCTION

The identification of active species for desired chemical reactions is a main quest in the field of heterogeneous catalysis.<sup>1</sup> Whether a species is active or not depends on many factors, including the nature of its interaction with the catalyst material, as well as the temperature and pressure at which the catalytic reactions take place. The main approach for gaining quantitative, microscopic understanding of various properties and processes, has been to perform experiments under standard surface science conditions, i.e., under ultra high vacuum (UHV) and relatively low (room or lower) temperatures, with the hope that what is learnt may be relevant and/or extrapolated to the system under the “real” catalytic conditions of high temperatures and pressures. Theoretical studies of adsorption and reactions at surfaces have, at best, been carried out by first-principles approaches, which, while highly accurate, typically do not take into account the temperature or the gas-phase environment with which the surface is in contact. A recent focus, both experimentally and theoretically, is to attempt to study systems which more closely resemble those of true catalytic ones.<sup>2</sup> Experimentally, this is done by performing *in situ* real-time measurements carried out under high temperature

and pressure conditions, and by the systematic study of, e.g., well-characterized metal clusters deposited on support materials and chemical reactions thereon (see e.g., Refs. 3,4,5,6,7,8). Such studies are important in particular for understanding those systems which exhibit a “pressure- and/or materials-gap”, i.e., where different behavior is exhibited under low and high pressures, or when results for model single-metal catalysts do not represent those of the “real” catalyst, typically consisting of a dispersed metal on a support material. Often the pressure- and materials-gaps are related and occur simultaneously.

The oxygen–silver system is an example which exhibits a pronounced pressure-dependence: Despite its unique activity as *the* catalyst for ethylene epoxidation ( $\text{C}_2\text{H}_4 + \frac{1}{2}\text{O}_2 \rightleftharpoons \text{C}_2\text{H}_4\text{O}$ , performed at 500-600 K and atmospheric pressure) and partial oxidation of methanol to formaldehyde ( $\text{CH}_3\text{OH} + \frac{1}{2}\text{O}_2 \rightleftharpoons \text{CH}_2\text{O} + \text{H}_2\text{O}$  - “oxydehydrogenation”, or by direct dehydrogenation,  $\text{CH}_3\text{OH} \rightleftharpoons \text{CH}_2\text{O} + \text{H}_2$ , performed at 700-900 K and atmospheric pressure), these reactions do not occur with any significant probability under UHV conditions.<sup>9,10,11</sup> This behavior of the oxygen–silver system might be related to a materials-gap, because for studies of the partial oxidation of methanol, drastic differences are observed in the performance for fresh silver catalysts and those which

have been exposed to high temperature ( $T > 873$  K) and pressure (atmospheric) conditions. The temperature dependence of the conversion of the clean Ag material to the active catalyst exhibits a pronounced hysteresis, i.e., the conversion is different when raising the temperature from low to high, compared to from high to low. This was the case for high temperatures up to 873 K, as well as for lower temperatures up to 560 K and 750 K. These hysteresis effects were shown from scanning electron microscopy (SEM) studies to be related to significant morphological changes which occur in the catalyst depending on the temperature, and that do not revert to the original structure when lowering the temperature, i.e., the changes are irreversible.<sup>12</sup> Structural changes in silver also occur when in contact with a *pure* O<sub>2</sub> environment at high temperatures ( $\sim 900$  K) and atmospheric pressure, namely, facets with the Ag(111) orientation result.<sup>12,13</sup> This is presumably because under these conditions it is unlikely that there will be any oxygen on the surface and the (111) surface of Ag has the lowest surface energy.

It has been suggested that the elusive sub-surface or “bulk-dissolved” oxygen species play an essential role in the above-mentioned catalytic reactions, which so far have escaped a precise characterization.<sup>12,13,14,15,16,17</sup> In addition to this aspect, there are other controversial debates in the literature concerning the nature of the active species, e.g., atomic versus molecular (ozone-like) oxygen.<sup>18,19</sup> Another puzzling issue is how silver, as a noble metal, can function as a good catalyst when it only binds adparticles relatively weakly on the surface compared to the transition-metal catalysts to the left of it in the periodic table. Catalysis clearly involves a number of complex processes, namely the dissociation of molecules and the creation of chemically active species, and subsequent interaction and reaction between the particles to form the product, which desorbs from the surface. Furthermore, it is possible (maybe likely) that some fragments of the reactant molecules (e.g., H or C) modify the catalyst material and thereby participate in the creation of the active species. In the present paper we tackle only part of the problem, namely, the study of the interaction of silver with oxygen in order to identify and exclude possible active O species for the above-mentioned heterogeneous catalytic reactions. This is an essential prerequisite for modeling the full catalytic process.

Although we study explicitly the (111) surface of silver, our general findings are expected to be relevant for silver *per se*, and possibly to have implications for gold, also a noble metal oxidation catalyst<sup>20</sup> which, for the (111) surface, exhibits a restructuring and chemisorption of oxygen atoms at elevated temperatures (500–800 K) and atmospheric pressure,<sup>21,22</sup> similar to Ag(111). They may also relate to copper, which catalyses the oxidation of methanol to formaldehyde.<sup>23</sup>

In our previous publications,<sup>24,25</sup> the interaction between oxygen and Ag(111) was thoroughly studied by density-functional theory (DFT). In these works we considered almost all possibly relevant oxygen species,

namely, pure on-surface chemisorbed oxygen, pure sub-surface and bulk-dissolved oxygen, surface- and bulk-substitutional adsorption, structures involving both oxygen on and under the top Ag layer, as well as surface-oxides and a molecular (ozone-like) species adsorbed at a surface vacancy. We studied these oxygen species for a wide range of coverages where the following results were obtained: At low coverages oxygen atoms adsorb on the surface. With increasing coverages, however, strong repulsive interactions develop between the partially negatively charged O atoms and the adatoms are driven to penetrate into the sub-surface region, and/or to give rise to a reconstructed, thin surface-oxide layer, when the coverage is larger than  $\sim 0.25$  ML. For higher oxygen contents, thicker oxide-like films are predicted to form.

We also found that the presence of sub-surface oxygen when bonded to the same surface Ag atoms as an oxygen atom on the surface, dramatically modifies the electronic properties of the on-surface oxygen and vice-versa. Depending on the particular geometry, it can give rise to a notable stabilization or destabilization, but the energetically favorable structures induce a *stabilization* and a lowering of the density of states at the Fermi level. In contrast to the conclusions concerning the crucial role of bulk-dissolved oxygen based on interpretations of experimental results, we found that this species is energetically *unfavorable*, as is bulk- and surface-substitutional oxygen, as well as the molecularly adsorbed ozone-like species at a vacancy, when the system is in thermal equilibrium.<sup>24,25</sup> On the other hand, the binding energy of atomic oxygen adsorbed at under-coordinated silver atoms is considerably stronger than on the terraces, but the concentration of such species obviously depends on the number of defects and the morphology of the substrate.

Nevertheless, temperature and pressure can affect the stability of structures and this has not been investigated so far. Clearly this is important for gaining an understanding of the system under catalytic conditions and this is the main topic of the present paper. Some of these results were reported briefly in Ref. 26. Our study uses the approach of “*ab initio*, atomistic thermodynamics”, that is, performing systematic DFT calculations for all O species that could conceivably be relevant, and take into account the effect of the environment, which we do via the pressure and temperature dependence of the oxygen chemical potential (see, e.g., Refs. 27,28,29,30,31,32). From the resulting free energies (obtained using our previously obtained energetics<sup>24,25</sup>), we derive the phase diagram of oxygen at the silver (111) surface. Since our earlier studies<sup>24,25</sup> predict that oxide-like structures form for high O concentrations, we also investigate the surface and bulk properties of the most stable bulk oxide, namely, di-silver oxide, Ag<sub>2</sub>O.

The paper is organized as follows: The calculation procedure, as well as the thermodynamical method are explained in Sec. II, and in Sec. III results are presented for the bulk properties of Ag<sub>2</sub>O. In Sec. IV, we investi-

gate various terminations of the  $\text{Ag}_2\text{O}(111)$  surface as a function of the oxygen chemical potential. Section V describes investigations into the transition from oxide-like structures (where the positions of the Ag atoms are commensurate with those of the  $\text{Ag}(111)$  substrate) to the true oxide film which is laterally expanded in comparison. In Sec. VI, the pressure–temperature phase diagram of the oxygen–silver system is presented and compared to experimental results. Finally, the conclusions are given in Sec. VII.

## II. CALCULATION METHOD

The DFT total-energy calculations are performed using the pseudopotential plane wave method<sup>33</sup> within the generalized gradient approximation (GGA).<sup>34,35</sup> The pseudopotentials are generated by the scheme of Troullier and Martins with the same functional.<sup>36,37</sup> The wave functions are expanded in plane waves with an energy cutoff of 50 Ry. In the  $(1 \times 1)$  surface unit cell, corresponding to the periodicity of clean  $\text{Ag}(111)$ , 21 special  $\mathbf{k}$ -points are used in the surface irreducible Brillouin zone (IBZ) for the Brillouin-zone integration.<sup>38</sup> Equivalent  $\mathbf{k}$ -points to these are used for all of the surface structures studied for consistency, i.e., to maximize the accuracy when comparing the energetics of different coverages as calculated in different supercells. We employ a Fermi function with a temperature broadening parameter of  $k_{\text{B}}T^{\text{el}} = 0.1$  eV to improve the convergence, and the total energy is extrapolated to zero temperature. ( $k_{\text{B}}$  is the Boltzmann constant.) The structures are created on one side of the slab and the resulting induced dipole moment is taken into account by applying a dipole correction.<sup>39</sup> For the adsorption structures on  $\text{Ag}(111)$ , we use five layers of Ag to model the surface and typically keep the bottom two or three layers fixed at the bulk-like positions and fully relax all the other atoms until the forces on the atoms are less than  $0.015$  eV/Å. The oxide surfaces of  $\text{Ag}_2\text{O}(111)$  are simulated by symmetrical slabs (i.e., with inversion symmetry). We tested thicknesses corresponding to five, seven, and nine metal layers, separated by  $15$  Å of vacuum. Our results show that the systems can be safely described using five metal layers with inversion symmetry.

In *ab initio* theory, the consideration of high temperature and high pressure can be achieved by explicitly taking into account the surrounding gas phase in terms of “*ab initio*, atomistic thermodynamics” (cf. e.g. Refs. 27,28,29,30,31,32). This is also an appropriate (first) approach to steady-state catalysis, which is often run close to thermodynamic equilibrium (or a constrained equilibrium) to prevent catalyst degradation. In the following we outline how the combination of thermodynamics and DFT can be applied to obtain the lowest-energy surface structures with a surrounding gas phase, thus enabling us to construct a  $(T, p)$ -diagram of the stability (or metastability) regions of different surface

phases.

We consider a surface in contact with an oxygen atmosphere which is described by an oxygen pressure  $p$  and a temperature  $T$ . The environment then acts as a reservoir, as it can give (or take) oxygen to (or from) the substrate without changing the temperature or pressure. We calculate the surface free energy,

$$\gamma(T, p) = (G - N_{\text{Ag}}\mu_{\text{Ag}} - N_{\text{O}}\mu_{\text{O}})/A \quad , \quad (1)$$

where  $N_{\text{O}}$  and  $N_{\text{Ag}}$  are the number of oxygen and silver atoms, and  $A$  is surface area. The  $T$  and  $p$  dependence is mainly given by  $\mu_{\text{O}}$ , the oxygen chemical potential, i.e., by the  $\text{O}_2$  gas phase atmosphere:

$$\mu_{\text{O}}(T, p) = 1/2[E_{\text{O}_2}^{\text{total}} + \tilde{\mu}_{\text{O}_2}(T, p^0) + k_{\text{B}}T \ln \left( \frac{p_{\text{O}_2}}{p^0} \right)], \quad (2)$$

where  $p^0$  corresponds to atmospheric pressure and  $\tilde{\mu}_{\text{O}_2}(T, p^0)$  includes the contribution from rotations and vibrations of the molecule, as well as the ideal-gas entropy at 1 atmosphere. It can be calculated or taken from experimental values from thermodynamic tables – the difference between theory and experimental values is marginal in the temperature range of interest. The silver chemical potential is

$$\mu_{\text{Ag}} = \begin{cases} g_{\text{Ag-bulk}}, & \text{for adsorption on a silver substrate} \\ \frac{1}{2}(g_{\text{Ag}_2\text{O-bulk}} - \mu_{\text{O}}), & \text{when bulk Ag}_2\text{O is present} \end{cases} \quad (3)$$

We use small symbols ( $g_{\text{Ag-bulk}}$ ,  $g_{\text{Ag}_2\text{O-bulk}}$ ) in Eq. 3 to indicate that these are free energies per Ag atom (top) and per  $\text{Ag}_2\text{O}$  unit (bottom). These two quantities are calculated by DFT-GGA. In Eq. 1, we have furthermore,

$$G = \begin{cases} G^{\text{slab}}, & \text{to obtain surface energies} \\ G_{\text{O/Ag}(111)}^{\text{slab}} - G_{\text{Ag}(111)}^{\text{slab}}, & \text{to obtain adsorption energies on Ag}(111) \end{cases} \quad (4)$$

These quantities are also calculated by DFT-GGA. For the temperature dependence of  $\tilde{\mu}_{\text{O}_2}(T, p^0)$ , we use thermodynamic tables [Ref. 40] (i.e., experimental data), while the  $T = 0$  K value of Eq. 2 is

$$\mu_{\text{O}}(T = 0\text{K}, p) = \frac{1}{2}E_{\text{O}_2}^{\text{total}}$$

$$\simeq E_{\text{Ag}_2\text{O-bulk}}^{\text{total}} - 2E_{\text{Ag-bulk}}^{\text{total}} + H_{\text{Ag}_2\text{O-bulk}}^f \quad (5)$$

In the above equation we use the experimental value of the heat of formation,  $H_{\text{Ag}_2\text{O-bulk}}^f$ , because of its very small value (0.323 eV at the standard state (room temperature and atmospheric pressure),<sup>41</sup> or 0.325 eV extrapolated back to  $T \rightarrow 0$  K), which implies that the error introduced in the later discussion by using the theoretical value (0.092 eV) would be significant. We note that the error in  $H_{\text{Ag}_2\text{O-bulk}}^f$  is due to the significant overbinding of  $\text{O}_2$ , and the underbinding obtained for bulk Ag and bulk  $\text{Ag}_2\text{O}$ .

We choose the zero reference state of  $\mu_{\text{O}}(T, p)$  to be the total energy of oxygen in an isolated molecule, i.e.,  $\mu_{\text{O}}(\text{OK}, p) = \frac{1}{2} E_{\text{O}_2}^{\text{total}} \equiv 0$ . This will be called the “oxygen-rich” condition. The so-called “oxygen-poor” value of  $\mu_{\text{O}}$  is taken as,

$$\mu_{\text{O}}^{\text{poor}} = E_{\text{Ag}_2\text{O}-\text{bulk}}^{\text{total}} - 2 E_{\text{Ag}-\text{bulk}}^{\text{total}}. \quad (6)$$

If the oxygen chemical potential becomes lower (more negative) than  $\mu_{\text{O}}^{\text{poor}}$ , di-silver oxide starts to decompose. For oxides of different transition metals, the “oxygen poor” limit can vary significantly depending on the heat of formation. For example, what may be rather “oxygen rich” for  $\text{RuO}_2$  (with  $H_f = 1.60$  eV) is already too “oxygen poor” for  $\text{Ag}_2\text{O}$  to be stable. The typical range of the allowed oxygen chemical potential is determined and limited by the pressures and temperatures used in industry and laboratories, namely, from several to thousand Kelvin, and from ultra high vacuum ( $< 10^{-12}$  atm.) to several hundreds of atmospheres.

For our investigations into various terminations of  $\text{Ag}_2\text{O}(111)$  surfaces, we will also consider the energy required to remove an oxygen atom from the surface and bring it to the vacuum. We call this the “removal energy”, and it is defined as,

$$E^{\text{removal}} = -E_{\text{O}/\text{Ag}_2\text{O}(111)} + (E_{\text{Ag}_2\text{O}(111)}^{\text{ref}} + E_{\text{O}}) \quad , \quad (7)$$

where  $E_{\text{O}/\text{Ag}_2\text{O}(111)}$  is the total energy of the surface termination of interest, containing the O atom to be removed,  $E_{\text{Ag}_2\text{O}(111)}^{\text{ref}}$  is that of the reference system, i.e., the surface structure remaining after the O atom has been removed.  $E_{\text{O}}$  is the total energy of a free O atom where the spin-polarization energy ( $-1.60$  eV) is taken into account. The removal energy reflects the bondstrength of the removed O atom to the surface.

To help analyze the electronic structure, we also calculate the density of states,  $N(\epsilon)$ , as well as the state-resolved DOS, or projected DOS,  $N_{\alpha}(\epsilon)$ . The definitions are given in Ref. 42.

### III. BULK $\text{Ag}_2\text{O}$

The most stable silver oxide is  $\text{Ag}_2\text{O}$ , which decomposes at 460 K under atmospheric pressure.<sup>41</sup> The crystallographic structure of di-silver oxide,  $\text{Ag}_2\text{O}$ , is shown in Fig. 1a. It has the cuprite structure with six atoms per cubic unit cell, (two oxygen atoms and four silver atoms) where the oxygen atoms form a body centered cubic lattice, while the metal atoms are located on the vertices of a tetrahedron around each oxygen atom, forming a face-centered-cubic lattice.<sup>44</sup> A characteristic feature, as seen in Fig. 1a, is a linear oxygen-metal-oxygen coordination. The calculations for  $\text{Ag}_2\text{O}$  are performed with 35 special  $\mathbf{k}$ -points in the irreducible part of the Brillouin zone (IBZ) of the six atom cell, corresponding to 1000 points in the full BZ. We used the same pseudopotentials and energy cut-off (50 Ry) as in our earlier works.<sup>24,25</sup>

TABLE I: Calculated DFT-GGA and experimental bulk properties of  $\text{Ag}_2\text{O}$ . The lattice constant,  $a_0$ , the distance between Ag atoms,  $d_{\text{Ag}-\text{Ag}}$  and oxygen atoms,  $d_{\text{O}-\text{O}}$ , and the bondlength between nearest neighbor oxygen and silver atoms,  $b_{\text{O}-\text{Ag}}$ , are given in Å. The bulk modulus,  $B$ , (in Mbar), and the heat of formation,  $H_{\text{Ag}_2\text{O}-\text{bulk}}^f$ , (in eV per oxygen atom) are listed as well.

	$a_0$	$d_{\text{Ag}-\text{Ag}}$	$d_{\text{O}-\text{O}}$	$b_{\text{O}-\text{Ag}}$	$B$	$H_{\text{Ag}_2\text{O}-\text{bulk}}^f$
Exp.	4.72 <sup>a</sup>	3.34 <sup>a</sup>	4.09 <sup>a</sup>	2.04 <sup>a</sup>	-	0.323 <sup>c</sup>
	4.74 <sup>b</sup>	3.35 <sup>b</sup>	4.10 <sup>b</sup>	2.05 <sup>b</sup>	-	-
Theory	4.91	3.47	4.25	2.13	0.647	0.092

Reference 43; <sup>b</sup> Reference 44; <sup>c</sup> Reference 41.

The calculated results, as well as available experimental data, are presented in Tab. I. The theoretical lattice constant of 4.91 Å is 4% larger than the experimental one which is 4.74 Å<sup>44</sup> or 4.72 Å.<sup>43</sup> The nearest-neighbor distance between Ag atoms in  $\text{Ag}_2\text{O}$  is calculated to be 3.47 Å, which is larger than the (theoretical) value in bulk fcc silver which is 2.97 Å. The calculated O-Ag bondlength is slightly shorter than for oxygen chemisorbed on the Ag(111) surface (compare 2.13 Å to 2.15-2.18 Å, depending on the coverage), and similar to the O-Ag bondlengths of the  $(4 \times 4)$  structure (depicted in Fig. 3 (bottom), discussed later and in Ref. 25) which are 2.10-2.11 Å for the upper O-Ag bonds and 2.14-2.16 Å for the lower O-Ag bonds (involving the surface Ag atoms). It is also similar to the O-Ag bond lengths of the favorable on-surface+sub-surface commensurate oxide structures (2.10-2.15 Å) reported in Ref. 25 [see e.g., the upper O-Ag-O layer of Fig. 3 (top)].

The calculated heat of formation, obtained as the total-energy difference between di-silver oxide ( $\text{Ag}_2\text{O}$ ) and the sum of the total energies of bulk silver (two Ag atoms) and the oxygen molecule (one O atom) is 0.092 eV. The difference to the experimental value of 0.231 eV is due to the significant overbinding of  $\text{O}_2$ , which is 0.566 eV per oxygen atom, and the underbinding obtained for bulk Ag and bulk  $\text{Ag}_2\text{O}$ . This leads to some cancellation of errors but it is not complete. In table I, the calculated bulk modulus refers to the theoretical lattice constant. To the best of our knowledge, there are no theoretical values of the heat of formation with which to compare in the literature, nor lattice constants or bulk moduli. Both experiment and theory, nevertheless, show that formation of di-silver oxide is an exothermic process, and the small value is in-line with the low temperature of decomposition noted above. The heat of formation of di-silver oxide is significantly smaller compared to the transition metal oxides for metals to the left of Ag in the periodic table, e.g. 1.60 eV, 1.19 eV, and 0.97 eV per oxygen atom (experimental data at  $T \rightarrow 0$  K and atmospheric pressure) for  $\text{RuO}_2$ ,  $\text{Rh}_2\text{O}_3$  and  $\text{PdO}$ , respectively.<sup>41</sup>

The total density of states is shown in the right panel of Fig. 1b. The peak located in the energy range  $-4.0$  to  $-2.0$  eV with respect to Fermi energy arises mainly

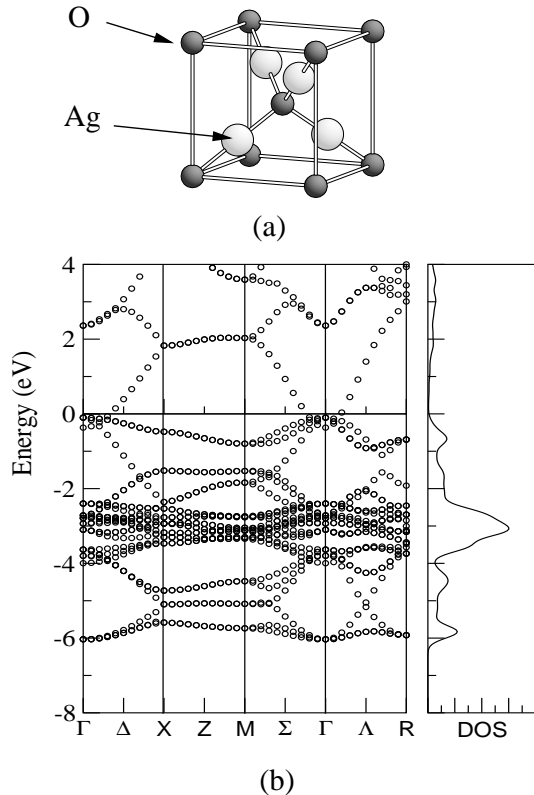


FIG. 1: (a) The cuprite structure of bulk Ag<sub>2</sub>O. The oxygen and silver atoms are indicated by the dark and pale grey circles, respectively. (b) The band structure of Ag<sub>2</sub>O calculated at the theoretical lattice constant (left), and the corresponding density of states (DOS) is shown at the right. The energy zero corresponds to the Fermi level.

from the Ag-4d states, where there is only a small overlap with the O-2p band, which has main (but smaller) peaks in the regions of  $-6$  to  $-4$  eV and  $-2$  to  $0$  eV. The states in the former region are largely bonding and those in the latter are mainly antibonding in character, as determined by inspecting the spatial distribution of the wave-functions in these regions. The occupation of the antibonding states, and small overlap of O and Ag states, explains the low stability of the oxide.

The band structure of Ag<sub>2</sub>O is shown in the left panel of Fig. 1b. It can be seen that at the  $\Gamma$  point, the valence and conduction bands overlap, making Ag<sub>2</sub>O metallic, instead of semiconducting with a band gap of  $1.3$  eV<sup>45</sup> as found in experiments. The spatial distribution of the wavefunctions in the conduction band close to the Fermi energy (investigated for several  $\mathbf{k}$ -points), shows that the states are of antibonding nature, involving a hybridization of Ag-4d-O-2p- and Ag-4d-O-3s-like orbitals. The occupation around  $\Gamma$  of these bands could contribute to the underestimate of the heat of formation of Ag<sub>2</sub>O noted above. We note, however, that this down shift of the conduction band has only a small effect on the DOS (cf. right

panel of Fig. 1b at energy  $\epsilon = 0$ ). We also performed calculations using the slightly smaller experimental lattice constant; this also did not yield a band gap. Using the augmented-spherical wave (ASW) method with an extended basis set and the atomic sphere approximation (ASA) within the local-density approximation (LDA), Czyzyk *et al.*<sup>46</sup> calculated the projected density of states and band structure of Ag<sub>2</sub>O, where a band gap  $0.40$  eV was found. However, no band gap was obtained by Deb and Chatterjee<sup>47</sup> using the full-potential linearized augmented plane wave (FP-LAPW) method within the local-spin density approximation (LSDA). Their reported density of states and band structure are very similar to those of our present work. In both of the two above-mentioned works, the lattice constant was not stated, but we believe the experimental one was used because our results calculated at the experimental lattice constant agree more closely. On increasing the energy cut-off and using harder pseudopotentials, namely,  $r_s = r_d = 2.20$  Bohr and  $r_p = 2.10$  Bohr for silver and  $r_s = r_p = r_d = 1.2$  Bohr for oxygen, and an energy cut-off of  $90$  Ry, no significant change in the results was found (less than  $0.02$  eV for the heat of formation,  $0.01$  Å for the lattice constant, and  $0.001$  Mbar for the bulk modulus). Thus it appears that Ag<sub>2</sub>O is another semiconductor for which the LDA and GGA yield no band gap. Other materials for which this is the case are, for example, Ge,<sup>48</sup> InN,<sup>49</sup> and ScN.<sup>50</sup>

Calculations for Ag<sub>2</sub>O performed using the screened-exchange local-density approximation,<sup>51</sup> which affords a more accurate description of the band-gap compared to the LDA (or GGA), yield a band-gap of  $0.73$  eV which shows that this material is indeed a direct narrow band-gap semiconductor, in agreement with experiment.

#### IV. Ag<sub>2</sub>O(111) TERMINATIONS

In this section, we examine various surface terminations of Ag<sub>2</sub>O(111). This is interesting for two reasons, firstly in relation to learning more about oxide surfaces in general through comparison with existing studies, and secondly since our earlier works<sup>24,25</sup> for oxygen adsorption at the Ag(111) surface predicted that for high oxygen concentrations, thick oxide-like structures form which contain half a monolayer of O between the Ag layers and quarter of a monolayer on the surface (see e.g., Fig. 3, upper right). On inspection of the geometry, we observe that the structures correspond exactly to that of the Ag<sub>2</sub>O(111) surface, but where the positions of the Ag atoms are commensurate with those of the underlying Ag(111) substrate, so the structure is laterally compressed compared to the true oxide [compare Figs. 2 and 3 (upper)]. With respect to different terminations, additional oxygen could adsorb on top of the Ag atoms. Such sites are called coordinatively unsaturated sites (“cus”), since compared to in the bulk, they are lacking their full O-coordination; for the present system, the cus Ag atoms are missing one O bond. Conversely, it could be favorable

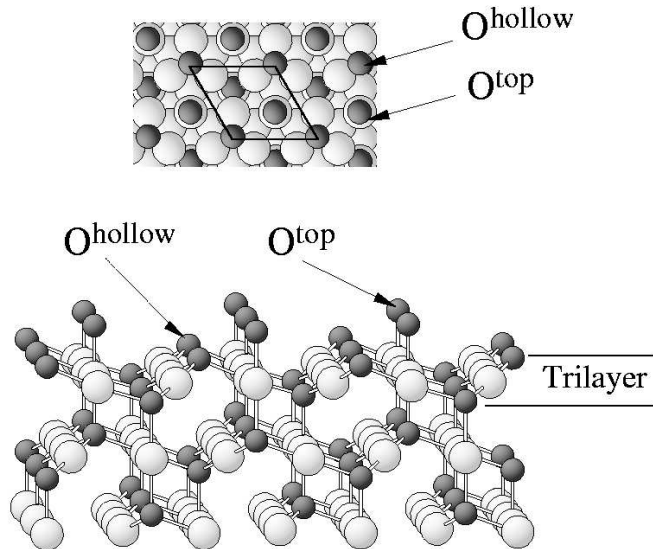


FIG. 2: Top (upper) and perspective (lower) views of the atomic geometry of the  $\text{Ag}_2\text{O}(111)$  surface. The silver atoms are represented by large, pale spheres and the oxygen atoms by small, dark spheres. The hollow and top sites of surface oxygen atoms are indicated, as is the “O-Ag-O trilayer” which contains two O atoms and four Ag atoms per surface unit cell.

that the surface has a metal-atom termination instead. We have therefore studied several different terminations, and calculated the surface free energy as a function of the oxygen chemical potential (cf., Eq. 2) to determine which have the lowest energy.

Figure 2 shows the two surface O atoms: The hollow site corresponds to the bulk stacking and the O atom in the top site makes this termination oxygen rich (without the  $\text{O}^{\text{top}}$  atoms the site would be a “cus” site). The silver-terminated surface is that where both of these O atoms are missing. The stoichiometric surface can be thought of as a stacking of O-Ag-O trilayers as indicated in Fig. 2, which contains two O atoms and four Ag atoms per unit cell of the layer. We investigated the surfaces with oxygen in the hollow site, and the oxygen-terminated surface with oxygen atoms in the hollow and top sites. We also tested the silver terminated surface, as well as a termination with oxygen atoms just in the top sites.

The surface free energies of the considered surface terminations are shown in Fig. 4. The range of the chemical potential between the vertical lines corresponds to the (experimental) heat of formation of  $\text{Ag}_2\text{O}$ , which is 0.325 eV, i.e. to the range in which bulk di-silver oxide is stable. It is clear that the surface with oxygen in the hollow site is the most stable one throughout the *whole range* of the chemical potential. The O terminated surface is very unfavorable. This is paralleled by the very large increase in the work function (by 2.84 eV with respect to the Ag-terminated surface, or 2.50 eV with respect to the stoichiometric surface with O in the hollow

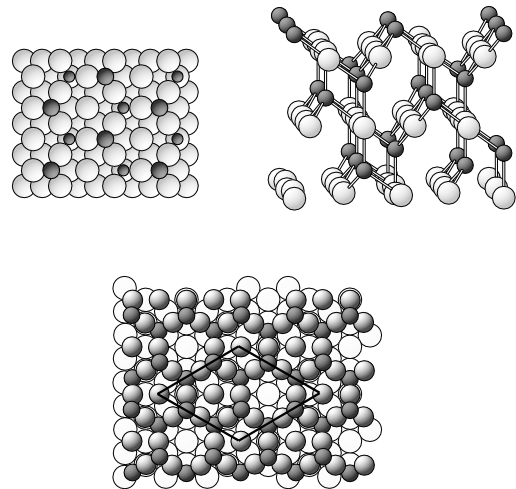


FIG. 3: Illustration of the atomic geometry of an oxide-like structure commensurate with the  $\text{Ag}(111)$  surface. Top view (upper left) and perspective view (upper right) for an O concentration of 1.25 ML. Ag atoms and O atoms are represented by large pale and small dark spheres, respectively. The structure is very similar to the true oxide (Fig. 2), but laterally compressed in comparison. Lower figure: sketch of the atomic structure proposed in the STM study of Ref. 52 for the  $(4 \times 4)$  oxygen phase on  $\text{Ag}(111)$ . The surface unit cell is indicated. The oxygen atoms are represented by small dark circles, the uppermost Ag atoms by grey circles, and the intact plane of  $\text{Ag}(111)$  atoms lying below the “O-Ag-O” trilayer are represented as the white circles. Note that this surface structure is the same as a layer of  $\text{Ag}_2\text{O}(111)$ , except there is one Ag atom missing in the indicated cell, which would sit directly on top of the Ag atom in the  $(111)$  surface below (which is energetically unfavorable).

sites). Such a large work function increase indicates that the O atoms have a significant negative charge, and so there will be a considerable O-O repulsion. The surface terminated with only O atoms in the top site is even less favorable than the fully O-covered surface.

The results described above are in contrast to those found for other (polar) oxide surfaces, e.g.  $\text{RuO}_2(110)$ <sup>32</sup> and  $\alpha\text{-Fe}_2\text{O}_3(0001)$ ,<sup>31</sup> where “full oxygen occupation” of available sites becomes favorable for high oxygen chemical potentials. The reason for this difference is because here the interaction between oxygen and silver is so weak that even extremely high values of the oxygen chemical potential cannot stabilize additional oxygen at the polar surface.

In Tab. II various physical properties of the surfaces are listed. In particular, it can be seen that the removal energy of O-hollow is greatest when there is no additional oxygen at the neighboring top site (compare 3.97 eV with 3.72 eV). Thus, the presence of O in the top site weakens the bond of the O-hollow atom to the surface, showing that there is a repulsive interaction between the O atoms in the hollow and top sites. We note that the value of

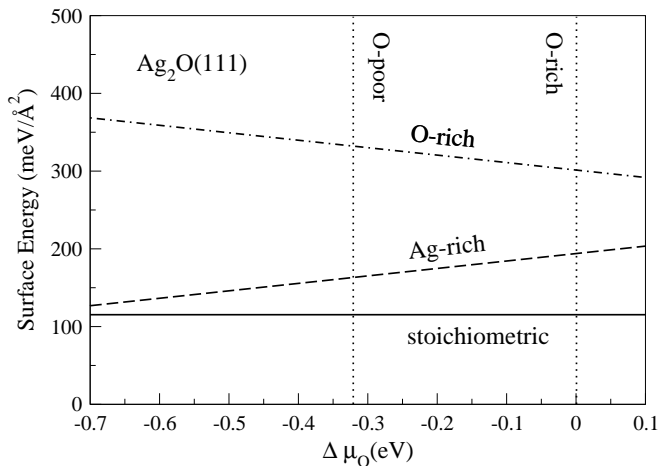


FIG. 4: Surface free energies,  $\gamma$ , as a function of the O chemical potential, for the various surface terminations of  $\text{Ag}_2\text{O}(111)$ : namely, Ag-terminated (dashed line), oxygen at the hollow site which corresponds to the stoichiometric surface (full line), and oxygen at both the hollow and top sites (dot-dashed line). The left and right vertical lines correspond to the “oxygen-poor-limit” and the “oxygen-rich-limit”, as explained in the text, and  $\Delta\mu_{\text{O}}$  is defined as  $\mu_{\text{O}} - 1/2E_{\text{O}_2}^{\text{total}}$ , using Eq. 5 for the latter.

3.97 eV is significantly stronger than 3.52 eV as obtained for O bonded to the clean Ag(111) surface in the fcc site at the same on-surface coverage of 0.25 ML as the O-hollow atoms shown in Fig. 2. It is, however, similar to the removal energies we found in our earlier work<sup>25</sup> for the energetically favorable structures involving both on-surface and sub-surface oxygen and the compressed oxide-like structures, where the values are in the range 3.90~4.01 eV. These bondstrengths can no longer be regarded as weak, but are intermediate – and of similar order as those identified for the reactive species involved in certain chemical reactions.<sup>53</sup>

### A. Atomic and electronic structure

The bondlength between oxygen in the hollow site and the surface silver atom for the energetically favorable  $\text{Ag}_2\text{O}(111)$  structure is 2.11 Å, which is slightly shorter than the corresponding bulk value (2.13 Å) noted in Sec. III. It is similar to that of the energetically favorable compressed oxide-like structures (2.10-2.15 Å) [see Fig. 3 (top)] which have a very similar local geometry, but smaller than that for chemisorbed on-surface oxygen at Ag(111) (2.15-2.18 Å), as found in our previous works.<sup>24,25</sup> The bondlength between oxygen in the top site and the silver atom below of 1.96 Å is significantly shorter because of its low coordination. Structurally, except for the Ag-terminated surface, where there is a large contraction of 10.3 % of the first metal interlayer spacing compared to that of the bulk truncated surface (calculated using the center of the layers), the relative

TABLE II: Physical properties of the various surface terminations for  $\text{Ag}_2\text{O}(111)$ .  $E_{\text{O-hollow}}^{\text{removal}}$  is the removal energy of the oxygen atom which occupies the hollow site for the two systems considered (cf. Eq. 7).  $\Delta d_{12}$  and  $\Delta d_{23}$  are the relative changes in the first two metal interlayer spacings with respect to the bulk value (2.83 Å),  $b_{\text{O-Ag}}$  is the bondlength of the surface oxygen atom to the uppermost metal atom, and  $\Phi$  is the work function. “O<sup>hollow</sup>” is the stoichiometric surface (O<sup>top</sup> removed, cf. Fig. 2) and “O<sup>full</sup>” denotes the structure shown in Fig. 2 where both O<sup>hollow</sup> and O<sup>top</sup> atoms are present.

System	$E_{\text{O-hollow}}^{\text{removal}}$ (eV/atom)	$\Phi$ (eV)	$\Delta d_{12}$ (%)	$\Delta d_{23}$ (%)	$b_{\text{O-Ag}}$ (Å)
Ag-term.	–	4.46	–10.3	1.8	–
O <sup>hollow</sup>	3.97	5.04	–0.6	–0.7	2.11
O <sup>full</sup>	3.72	7.30	–1.6	0.4	2.09 (hollow) 1.96 (top)

change in the metal interlayer spacings of the oxygen-terminated structures is modest, i.e., less than 2.0 %. For the stoichiometric surface, the rumpling of the silver atoms in surface metal layer is not negligible; the magnitude is of the order 0.10 Å. This is due an outward movement of the Ag atom in the surface unit cell that is not bonded to the surface O atoms, i.e., the “cus” atom. These relaxations are smaller than those of the “true transition-metal” oxides (i.e., with incomplete filling of the  $d$ -band), e.g.  $\alpha\text{-Fe}_2\text{O}_3(0001)$ <sup>31</sup> and  $\text{RuO}_2(110)$ ,<sup>32</sup> which we attribute to the weaker bonding between silver and oxygen. Similarly, for adsorption of oxygen on the Ag(111) surface, we found only very small relaxations of the substrate metal layers<sup>24</sup> in contrast to O on Ru(0001)<sup>54</sup> where the O-metal bond is notably stronger and oxygen adsorption induces a significant expansion of the first metal interlayer spacing. The nature of the bonding of the di-silver oxide surface is similar to that of the bulk oxide: Oxygen and silver hybridize mainly via the Ag-4*d*- and O-2*p*-like orbitals as shown in Fig. 5, where the atom projected density of states of the first O-Ag-O trilayer is shown. Compared to oxygen chemisorbed on the clean Ag(111) surface (see Fig. 5 in Ref. 24), the Ag-4*d* band is significantly narrower, which is due to the increased distance between the silver atoms and the weak hybridization with O-2*p* states. The PDOS in Fig. 5 is rather similar to that of the oxide-like structures with same local bonding as presented in Fig. 12 of Ref. 24. In Fig. 5 two features, one at –5.53 eV and one at –0.66 eV, with respect to the Fermi energy, can be seen which are well separated from the center of the  $d$ -band. This is in contrast to the case of chemisorption on the metal substrate, where there is only one peak outside of the Ag-4*d* band, for example at –1.35 eV for oxygen in the on-surface fcc-hollow site at coverage 0.25 ML.

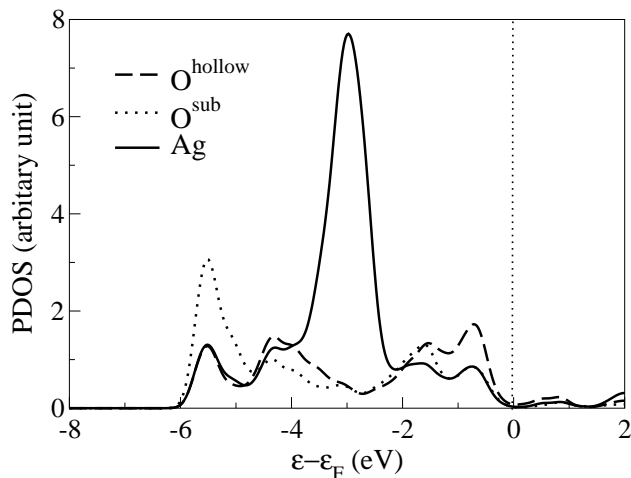


FIG. 5: Projected density of states (PDOS) of the first O-Ag-O trilayer (i.e., the stoichiometric surface): The surface oxygen (dashed line) which binds to three Ag atoms (it is also called hollow site oxygen). The Ag atom which is bonded to these  $O^{\text{hollow}}$  atoms (solid line), and the sub-surface oxygen atom bonded to this Ag atom as well as to a single Ag atom in the layer beneath (dot-dashed line) [see Fig. 2, ignoring the  $O^{\text{top}}$  atoms]. The energy zero is the Fermi energy, as indicated by vertical line.

## V. TRANSITION TO THE OXIDE

Having studied the atomic and electronic structure of bulk  $\text{Ag}_2\text{O}$  and determined the thermodynamically most favorable surface of  $\text{Ag}_2\text{O}(111)$ , we now wish to investigate how a transition from the oxide-like structures, with positions of Ag atoms commensurate with those of  $\text{Ag}(111)$ , and laterally compressed by 14 % compared to the true oxide (as reported in Ref. 25), to the real oxide structure might occur. Such a commensurate oxide-like structure is depicted in Fig. 3 (top) for an O concentration of 1.25 ML. In order to investigate such a transition, we study the difference of the total energy (per O atom) between oxide-like films (with commensurate Ag positions to those of the metal substrate) and corresponding “real” (unstrained) oxide layers as a function of thickness. Because the structures can be thought of as the stacking of O-Ag-O trilayers (see Fig. 2), we calculate the energy difference with increasing numbers of trilayers. Then the number of layers at which the true oxide structure becomes energetically more favorable, defines a critical thickness for the transition to occur. In this approach, the coupling between the (strained) oxide-like film with the underlying metal substrate is not included. We note that this study may be somewhat “academic” since there is so far no evidence for such compressed oxide structures, however, this structure is a plausible intermediate and perhaps can even be stabilized under certain experimental conditions. Furthermore, additional insight into the O/Ag system can be obtained by these calculations, and moreover, when compared to analogous

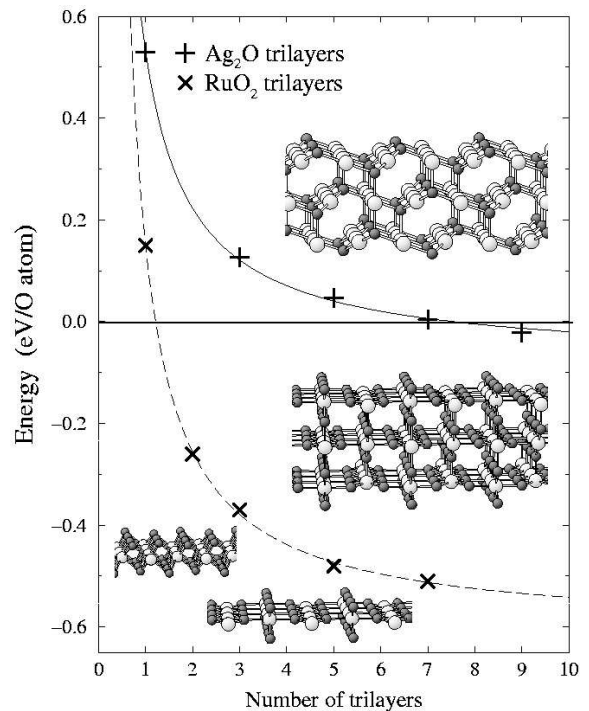


FIG. 6: Difference in total energy (per O atom) between a stack of O-Ag-O trilayers, commensurate with  $\text{Ag}(111)$ , and that of a corresponding oxide layer, as a function of the number of trilayers in the stack (denoted by “+”). The commensurate structures are just like the oxide, only laterally compressed by 14 % and vertically expanded by  $\sim 21$  %. A negative value indicates that the true oxide structure is energetically more favorable. For comparison, analogous results (from Ref. 55) are shown for  $\text{Ru}(0001)$  (denoted by “x”) namely, the difference in total energy (per O atom) between a stack of O-Ru-O trilayers [commensurate with  $\text{Ru}(0001)$ ] and that of corresponding  $\text{RuO}_2(110)$  layers as a function of layers in the stack. The lines connecting the Ag and Ru results (full and dashed lines) are guides to the eye. Insets illustrate the atomic geometry of the bulk oxide structures where oxygen and metal atoms are represented by small dark and large pale circles, respectively. For  $\text{RuO}_2$ , the O-Ru-O trilayer structure is also depicted (lower left), as well as its conversion, via an “accordian-like” expansion, into a “true”  $\text{RuO}_2(110)$  layer.

studies performed for other O/transition-metal systems, in particular for O/ $\text{Ru}(0001)$ ,<sup>55</sup> various trends may be identified.

The results are shown in Fig. 6. A negative value indicates that the true oxide structures are energetically more favorable. We note that Fig. 6 assumes that the number of O atoms is fixed. However, in many (most) experiments that aim to study very high coverages, the actual thermodynamic variable may be  $\mu_{\text{O}}$ .

For one O-Ag-O trilayer, the “strained” [commensurate with  $\text{Ag}(111)$ ] oxide film is significantly more favorable than the corresponding true oxide, as indicated by the relatively large positive value of 0.53 eV, but the



preference decreases quickly to 0.13 eV at three trilayers. On increasing the thickness further, the difference in the energy between the two structures decreases more slowly, and when the number of trilayers is nine, the true oxide film is energetically more favorable, as indicated by the negative value in Fig. 6. Because each trilayer contributes half a monolayer of oxygen, the critical coverage for the transition from the commensurate oxide-like film to the true oxide film is around 3.5-4.5 ML. As the number of the trilayers approaches infinity, clearly the curve approaches the value corresponding to the energy difference (per O atom) between the bulk oxide and the “strained” [commensurate with Ag(111)] bulk material.

The electronic properties of the “strained” [commensurate with Ag(111)] oxide film are very similar to those of the true oxide as can be seen from comparison of Fig. 12 in Ref. 25 with Fig. 5. This at first may be somewhat surprising since the lateral dimensions of the commensurate, oxide-like structures are smaller, by 14 %. We find, however, that much of the associated strain energy is relieved by expansion of the Ag layers perpendicular to the surface to accommodate the O atoms in between. Through this relaxation, the lattice volume per atom is 92 % of that of the bulk oxide.

In Fig. 6, analogous results for the phase transition from O-Ru-O trilayer structures (commensurate with Ru(0001)) to the corresponding real RuO<sub>2</sub>(110)<sup>55</sup> oxide layers are also presented for comparison. Bulk ruthenium dioxide has the rutile structure. The atomic geometry of RuO<sub>2</sub>(110) is shown as an inset in Fig. 6, as is that of the (commensurate) trilayer and its expansion into a corresponding true RuO<sub>2</sub>(110) layer (bottom, left). The commensurate trilayer structures are, laterally, 15 % and 35 % smaller than for RuO<sub>2</sub>(110) (i.e., in the  $\hat{a}$  and  $\hat{b}$  directions of the rectangular (110) surface unit cell). In this case the transformation from commensurate trilayer to corresponding oxide layer, involves not only a lateral expansion like for the di-silver oxide structures, but also a “rotation” of the O atoms about the Ru atoms, as seen from the inset (explained in more detail in Ref. 55). In particular, every second O-Ru-O component rotates to be horizontal to the surface, while the alternative components rotate so that they are perpendicular to the surface. In contrast to the Ag-O system, the phase transition into RuO<sub>2</sub>(110) oxide happens after only one O-Ru-O trilayer. Also, for Ru(0001), each trilayer contributes two monolayers of oxygen, so the critical coverage is around 2-4 ML. Because of the considerable energy gain due to formation of the real RuO<sub>2</sub> oxide layers, compared to continuous stacking of the O-Ru-O trilayers, the formation of the oxide structure will certainly take place once it is kinetically possible.

It is interesting to note that the energy differences of oxygen in the trilayers and the corresponding bulk metal oxide layers, exhibits a rather similar dependence on the number of layers for both O/Ag and O/Ru, except shifted in energy. This makes sense since we consider the energy per O atom, and as the stack becomes larger, there

are more and more O atoms in the center of the stack which have atomic environments which are similar (and thus similar energies), i.e., the affect on the energy due to the surfaces of the layers, diminishes. In view of this similarity, together with the fact that the heat of formation of e.g., the Rh (1.19 eV) and Pd (0.97 eV) oxides lie between the extremes of Ru (1.60 eV) and Ag (0.33 eV) oxides, we may expect that investigations of analogous transitions from commensurate structures to the bulk oxide phase for Rh and Pd would exhibit a behavior intermediate to those of Ru and Ag. This would imply the trend that the transition from intermediate, commensurate, two-dimensional oxide films to the true oxide phase, occurs sooner (i.e., for thinner films) for the elements more to the left in the periodic table, like Ru, with larger heats of formation, compared to those towards the right, which have smaller heats of formation like Ag.

From a recent trend study on the oxidation at the basal plane of late 4d transition metals (from middle to right in the periodic table, i.e., Ru, Rh, Pd, Ag),<sup>56</sup> it was found that oxygen starts to enter the sub-surface region only after a certain critical coverage has been reached on the surface. Namely, at coverages beyond which the heat of oxygen adsorption on the surface becomes unfavorable compared to the heat of formation of the bulk oxide. The reported critical coverages are about 1.0 ML, 1.0 ML, and 0.75 ML, and 0.25 ML for Ru, Rh, Pd, and Ag, respectively. Beyond these critical coverages, onset of bulk oxide formation was proposed to take place. Clearly, however, due to kinetic hindering, bulk oxide formation may *not* be able to occur “immediately” and then it may proceed via the formation of oxide-like layers as described above.

## VI. THERMODYNAMICS OF THE OXYGEN-SILVER(111) SYSTEM

We now turn to investigate the affect of the temperature and pressure on the stability of the various oxygen/silver structures, the energetics and atomic geometries of which were reported in our previous publications;<sup>24,25</sup> in particular, the energies are summarized in Fig. 14 of Ref. 25.

To incorporate the effect of temperature and pressure, we calculate the Gibbs free energy as a function of the oxygen chemical potential (cf., Eqs. 1 and 2) similarly to the oxide surfaces, except here the reference system is the clean metal substrate. As discussed above, the “oxygen poor” limit is that below which di-silver oxide is unstable. For oxygen adsorption at the Ag(111) surface, however, this limitation doesn’t necessarily exist. The results are shown in Fig. 7, where we only show the low energy structures. The dependence of the energy on  $\mu_{\text{O}}$ , namely the slope of the line, reflects the O coverage. The higher the coverage, the steeper the gradient. We also include the corresponding temperatures for two

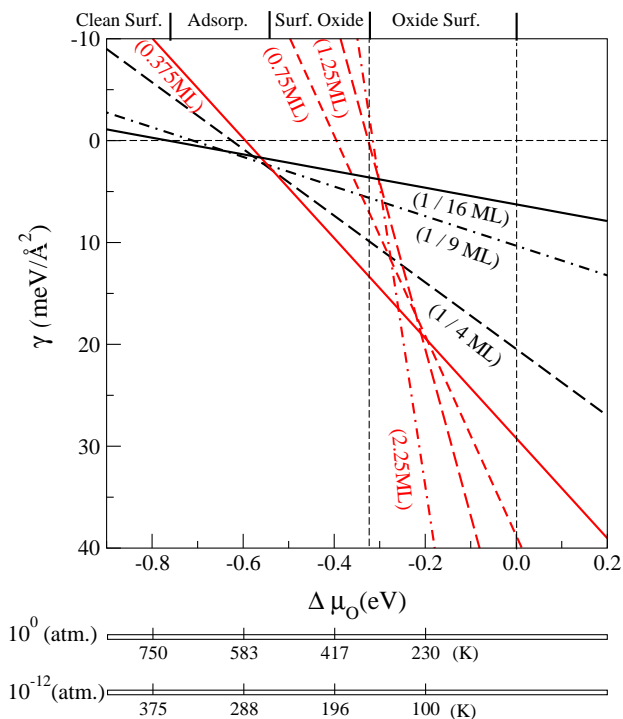


FIG. 7: Surface free energies for O at Ag(111) for the various low energy structures as a function of the O chemical potential, where  $\Delta\mu_{\text{O}}$  is defined as  $\mu_{\text{O}} - 1/2E_{\text{O}_2}^{\text{total}}$ , using Eq. 5 for the latter. On-surface chemisorbed oxygen with coverages 1/16 ML, 1/9 ML, and 1/4 ML (labeled by these coverages), the  $(4 \times 4)$  structure (accordingly labeled “0.375 ML”), commensurate oxide-like structures with coverages 0.75 ML, 1.25 ML, and 2.25 ML (as labeled by the coverages). The corresponding temperatures are given for two selected pressures (cf. Eq. 2), one corresponding to UHV conditions and the other to the atmospheric conditions of catalysis.

given pressures, namely, that which corresponds to UHV and the other characteristic of the atmospheric pressure employed in catalysis.

It can be seen that for low values of the oxygen chemical potential, i.e.  $< -0.78$  eV, the clean Ag(111) surface is thermodynamically most stable. For higher values, (i.e., in the range of  $-0.78$  eV to  $-0.63$  eV), a low coverage (1/16 ML) of oxygen on the surface in fcc-hollow sites is thermodynamically most stable, and for values greater than  $-0.63$  eV and less than  $-0.54$  eV, slightly higher coverages of adsorbed O (1/9 ML and 1/4 ML) become most stable. Increasing the oxygen chemical potential to values greater than  $-0.54$  eV leads to the formation of the reconstructed  $(4 \times 4)$  phase (labeled “0.375 ML”), which is stable up to  $\Delta\mu_{\text{O}} = -0.325$  eV, i.e. to the “O-poor” limit (left vertical dashed line), where the bulk oxide becomes stable. The atomic geometry of the  $(4 \times 4)$  phase is illustrated in Fig. 3 (bottom). The atomic structure is very similar to a trilayer of  $\text{Ag}_2\text{O}(111)$ , except with one Ag in the  $(4 \times 4)$  cell missing. The basis for this proposed structure (cf. Refs. 52,57,58,59,60) is the observation that the area of the  $(\sqrt{3} \times \sqrt{3})R30^\circ$ - $\text{Ag}_2\text{O}(111)$

surface unit cell is practically four times that of clean  $(1 \times 1)$ -Ag(111); the difference in the length of the lattice vectors is only 1.2% (0.3% from the experimental lattice constants). Although the mentioned *surface unit cells* are (practically) commensurate, the positions of the Ag atoms within the  $(\sqrt{3} \times \sqrt{3})R30^\circ$  oxide surface cell are, all except one, incommensurate with those of the Ag(111) surface.

It can be seen that for values of  $\Delta\mu_{\text{O}}$  greater than  $-0.54$  eV, the commensurate oxide-like structures (see e.g., Fig. 3) (top) are also quite favorable (labeled by the O coverages, 0.75, 1.25, 2.25 ML). It can be noticed that the thicker the film, the more stable the structure is (i.e., the steeper the curve). Clearly, in the limit of an infinitely thick film, the corresponding line would be very close to the left vertical one. This is so because the average O binding energy in the thick commensurate oxide-like structures is very similar to that of O in the bulk oxide as described above. From Fig. 7 it can be concluded that the bulk oxide is the thermodynamically most favorable structure once the oxygen chemical potential is higher than the “O-poor” condition, which is expected. However, the kinetics of oxide formation can be very slow and the thickness of the oxide film will be limited by O and metal bulk diffusion. Thus, it is unlikely that full thermal equilibrium of  $\text{O}_2$  with bulk di-silver oxide will be achieved.

### A. The O-Ag(111) phase-diagram

The results discussed above can be displayed as a continuous function of temperature and pressure by constructing a two-dimensional phase diagram, if we only consider the lowest energy structures. This has been done in Ref. 26 and the results are shown again in Fig. 8. Before giving a discussion, it is necessary to consider the magnitude of the error bars in the temperature and pressure. An indication can be obtained from knowledge of the stability of the bulk oxide, i.e., that it decomposes at 460 K under atmospheric pressure. From Figs. 7 and 8, the calculations predict that the bulk oxide decomposes at  $\sim 350$  K at atmospheric pressure, i.e., around 110 K lower than experiment. At 460 K, the bulk oxide is unstable when the pressure is lower than  $10^3$  atm., i.e., compared to 1 atm. as observed experimentally. The reason for this disparity may be due to *systematic* errors of the DFT-GGA approach and/or to neglect of the entropy contribution. In particular, we note that the experimental  $-TS$  contribution for bulk silver at 450 K and 1 atm. is  $-0.48$  eV per two silver atoms, and  $-0.70$  for  $\text{Ag}_2\text{O}$  per formula unit.<sup>41</sup> Thus, the entropy contribution from di-silver oxide, compared to silver bulk (the entropy of  $\text{O}_2$  has already been included in the chemical potential), is greater by 0.22 eV per two silver atoms, which will shift the left vertical line in Fig. 7 further to the left. Therefore, in Figs. 7 and 8, we generally expect that the temperature is underestimated, but the error less than

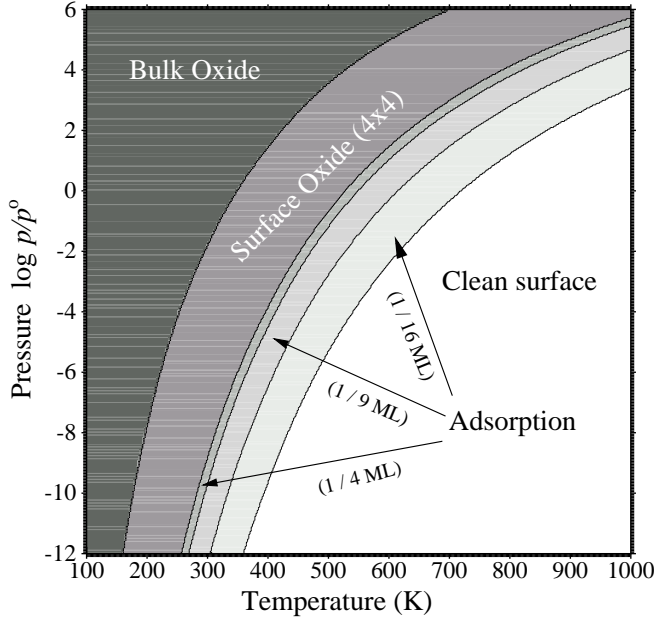


FIG. 8: Calculated phase-diagram for the oxygen-Ag(111) system. On the horizontal axis is the the temperature in Kelvin, and on the vertical axis is the pressure.

110 K, while correspondingly, the pressure is overestimated, by less than three orders of magnitude. For the temperature values quoted below, we give an estimate of the upper limit in brackets, that is, 110 K higher than that obtained from Fig. 8. In spite of these uncertainties, we believe that the relative stability of the various systems and our general understanding and conclusions will not be affected.

Typically, vibrational contributions to *differences* in the Gibbs free energies of extended systems exhibit some cancellation.<sup>32</sup> However, when there are additional atomic or molecular species which are not present in the reference system, the situation may be different as there will be no effective cancellation of the contributions of such species between surface and reference systems (as is the case using the *clean* Ag(111) as reference). We investigate this aspect in more detail for the present system; in particular, we consider low coverages of on-surface oxygen and thin oxide-like structures. We calculate the difference in the vibrational and entropic contributions to the Gibbs free energy,  $F^{\text{vib}} = E^{\text{vib}} - TS^{\text{vib}}$ , as,

$$\Delta F^{\text{vib}}(T, \omega) = \left\{ \hbar\omega \left( \frac{1}{2} + \frac{1}{e^{\beta\hbar\omega} - 1} \right) - k_B T \left[ \frac{\beta\hbar\omega}{e^{\beta\hbar\omega} - 1} - \ln(1 - e^{-\beta\hbar\omega}) \right] \right\}, \quad (8)$$

where  $\beta = 1/k_B T$  (see e.g. Ref. 28,32). The vibrations which enter Eq. 8 are those of the adsorbed O atoms. The calculated perpendicular vibrational frequency for 0.25 ML of oxygen in fcc sites on the surface is 50 meV ( $400 \text{ cm}^{-1}$ ), and we assume that the lateral vibrations are

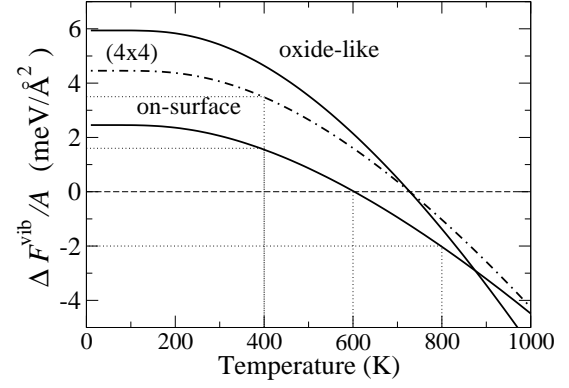


FIG. 9: Vibrational contribution (oxygen only, see text) to the Gibbs free energy,  $F^{\text{vib}}$ , for various adsorbate structures on Ag(111). i) The structure with a coverage of 0.25 ML of oxygen in fcc sites on the surface, ii) for the structure with one O atom in the fcc on-surface site and one O atom in the sub-surface tetrahedral site (labeled “oxide-like”), and iii) an estimate for the  $(4 \times 4)$  phase (dot-dashed line).

the same (this is a somewhat rough approximation but suffices for the present discussion, see below). Thus, in calculating  $\Delta F^{\text{vib}}(T, \omega)$  we multiply by a factor of three corresponding to these three modes. For the thin commensurate oxide-like structure containing one O atom on the surface in fcc sites and one sub-surface O in tetrahedral sites (i.e., a total coverage of 0.5 ML), the calculated perpendicular vibrational frequencies are 56 meV ( $455 \text{ cm}^{-1}$ ) and 65 meV ( $526 \text{ cm}^{-1}$ ), respectively, for these two species. Again, assuming each O atom has three modes equal to the perpendicular ones, we obtain the results presented in Fig. 9.

It can be seen from Fig. 9 that for on-surface O, for temperatures up to about 800 K, the contribution is a maximum of about  $\pm 2 \text{ meV}/\text{\AA}^2$ . For lower coverages of on-surface O such as the 1/16 and 1/9 ML structures, the contribution will be smaller (assuming the frequency is similar). For the oxide-like structure at coverage 0.5 ML, the effect is larger, namely  $5\text{--}6 \text{ meV}/\text{\AA}^2$  for temperatures up to about 400 K, thereafter decreasing. For the  $(4 \times 4)$  thin oxide structure with coverage 0.375 ML, we expect the vibrational frequencies of the O species will be similar to those of the structure at 0.5 ML since the local coordination of the O atoms is similar, as well as the electronic structure. In addition, the vibrational frequency of O in bulk  $\text{Ag}_2\text{O}$  is reported to be 66 meV ( $530 \text{ cm}^{-1}$ ),<sup>61</sup> which is very close to that of the O atom in the sub-surface tetrahedral site of the 0.5 ML coverage structure (65 meV). Because of the lower O coverage of the  $(4 \times 4)$  structure, the contribution to the free energy will be smaller than the 0.5 ML structure by about  $0.375/0.5 = 0.75$ , giving a maximum contribution at low temperatures of  $4.5 \text{ meV}/\text{\AA}^2$  (dot-dashed line in Fig. 9).

For the  $(4 \times 4)$  structure, in the temperature range

400 K to 730 K, it gives rise to a destabilization of less than  $3.5 \text{ meV}/\text{\AA}^2$  (the value at 400 K, which decreases with temperature), which on inspecting the energy scale of Fig. 7 can be seen to be non-negligible. The relative energy *difference*, however between the on-surface species and  $(4 \times 4)$  structure, which determines the *sequence* of the stable phases, can be seen from Fig. 9 to be affected by less than  $1.9 \text{ meV}/\text{\AA}^2$  ( $1.9 = 3.5 - 1.6 \text{ meV}/\text{\AA}^2$ ) for temperatures greater than 400 K, which will therefore have a small effect. We note that if the lateral vibrations would be 30 % greater than the perpendicular ones for the on-surface and oxide-like structures considered, this would result only in a small increase in the contribution to the free energy, i.e. of 0.5 and  $1.2 \text{ meV}/\text{\AA}^2$ , respectively, at  $T$  close to zero.

The above analysis may be regarded as qualitative, but it gives an estimate of the magnitude of the changes in the free energy due to consideration of vibrational and entropic effects of the extended systems for the energetically most important O/Ag structures. Clearly, for other systems with adsorbed species that have high frequencies such as OH (of the order 400 meV),<sup>62</sup> the contribution to the free energy from vibrational and entropic effects will be significantly greater and will have to be taken into account in determination of the phase diagram.

Summarizing the results contained in Fig. 8, we obtain the following predictions: Under UHV conditions ( $p = 10^{-12}$  atm.), chemisorption of oxygen on Ag(111) with low coverage (less than 0.0625 ML) is stable up to about 360 K (incl. corrections: 470 K). This is in-line with experimental results<sup>58</sup> where it has been found that for temperatures less than 490 K, 0.03 ML of oxygen can be adsorbed on the Ag(111) surface. Under UHV conditions, the calculations also predict the stability of the  $(4 \times 4)$  phase at the lower temperatures of 160 K (incl. corrections: 270 K) to 260 K (incl. corrections: 370 K). This is also consistent with scanning tunneling microscopy (STM) results obtained under UHV conditions at low (4 K) temperatures<sup>52</sup> where atomic resolution images of the  $(4 \times 4)$  phase have been achieved. The  $(4 \times 4)$  phase, however, cannot be directly prepared under these conditions as it is known from experiment that temperatures greater than 400 K are required in order for the necessary atomic rearrangement take place. It is therefore clear that it is the kinetics that prevent the reconstruction and formation of this phase at low pressures and temperatures. From Fig. 8, it can be seen that the  $(4 \times 4)$  phase should develop into the oxide if the oxygen pressure is raised or if the temperature is lower than 160 K (incl. corrections: 270 K). Such transitions, however, may be prevented or hindered by kinetics (e.g. diffusion barriers) since extensive mass transport is required to form the oxide.

At atmospheric pressure ( $p = 1$  atm.), typical of that used in industry, the bulk oxide is calculated to be only stable up to around 350 K (incl. corrections: 460 K). From this point of view, it can be concluded that for industrial reactions which take place at considerably higher

temperatures, di-silver oxide cannot be the active phase. The  $(4 \times 4)$  surface-oxide phase, however, is stable in the temperature range of 350-530 K (incl. corrections: 460-640 K) which coincides with that at which epoxidation of ethylene occurs. We therefore propose that such atomic O species are actuating the reaction. With regard to the catalytic reactions that take place at even higher temperatures, it can be seen that only very low coverages of chemisorbed O are stable up to 720 K (incl. corrections: 830 K); O atoms adsorbed at under-coordinated surface Ag atoms are up to 865 K (incl. corrections: 975 K) (see below). Therefore these species could possibly play a role in these reactions.

It is interesting to note that regardless of the pressure, Fig. 8 shows that the *ordering* of the stable phases is the same, so that the same phases should be observable at different pressures if the temperature is adjusted accordingly. This indicates a way to bridge the pressure gap, i.e., by appropriate choice of the pressure and temperatures to stay within the same phase. However, it is clear that sometimes this will not be possible within reasonable times because of kinetic hindering for dissociation and sticking of  $\text{O}_2$  (i.e., delivery of sufficient concentrations of atomic oxygen to the surface), as well as to kinetic limitations for adequate atomic rearrangement.

Experimentally, it has been reported that a “strongly bound” oxygen species (named  $\text{O}_\gamma$ ) forms after high temperature ( $\sim 900$  K) and atmospheric pressure exposure of polycrystalline silver, as well as Ag(111), to an oxygen environment.<sup>12,17</sup> Temperature programmed desorption spectra show that  $\text{O}_\gamma$  desorbs at around 900 K and it is proposed by the authors to be the active species for the dehydrogenation of methanol<sup>12,13</sup> where it diffuses to the surface from bulk sites. At the high temperature of  $\sim 900$  K in an oxygen atmosphere, silver reconstructs to form many (111) facets<sup>12,13</sup> at the surface and it is speculated that this means that oxygen diffusion takes place by a so-called “substitutional diffusion mechanism” which the authors argue has higher barriers than usual interstitial diffusion, and to give rise to the  $\text{O}_2$  desorption peak at the high temperature of 900 K. From our calculations, this picture is difficult to understand, in particular, how sufficient amounts of bulk-dissolved oxygen can be formed. From our theoretical study, we know that at lower coverage, oxygen will prefer to stay on the surface, instead of in the sub-surface or bulk region, and for high O concentrations, oxide-like structures are preferred.<sup>25</sup> Furthermore, our results showed that substitutional oxygen adsorption in the bulk (i.e., O on Ag sites) is energetically unfavorable.<sup>25</sup>

### B. O adsorption at under-coordinated metal sites: Ag vacancies

The importance of steps and vacancies as active sites has been well documented, from both experimental and theoretical points of view.<sup>63,64</sup> In our previous studies we

investigated the binding of oxygen atoms on surfaces with pre-existing vacancies.<sup>24</sup> We found the binding energy is stronger than on the (111) terraces, e.g., for 0.25 ML adsorbed in fcc sites on a  $(2 \times 2)/\text{Ag}(111)$  vacancy array the binding energy is 3.83 eV while it is 3.52 eV on the perfect terrace, at the same coverage. A similar behavior can be expected for adsorption at under-coordinated sites at step edges, as has been shown theoretically for oxygen at other transition metals, see e.g. Refs. 53 and 63. To investigate the affect of pressure and temperature on the stability of such O species, we calculated the Gibbs free energy of formation. We find that under atmospheric pressure, the O atoms are stable to around 770 K (incl. corrections: 880 K) on a  $(3 \times 3)/\text{Ag}(111)$  vacancy array, and even to 865 K (incl. corrections: 975 K) on a  $(2 \times 2)/\text{Ag}(111)$  vacancy array. The existence and concentration of these species, however, clearly depends on the number of defect sites at the surface. In view of the above, it could be speculated that the TPD signal of “O<sub>γ</sub>” is due not to substitutional diffusion of oxygen atoms from the bulk to the surface as proposed, but due to O atoms adsorbed at under-coordinated surface silver sites.

### C. Adsorption of O<sub>3</sub> at an Ag vacancy

As mentioned in the introduction, in the literature, the existence of surface Ag vacancies has been proposed to stabilize a molecular-like ozone (O<sub>3</sub>) species, which has been suggested to be active for the partial oxidation of ethylene.<sup>19</sup> As reported in Ref. 25, we calculated the adsorption energy of such a species on  $(3 \times 3)$  and  $(\sqrt{3} \times \sqrt{3})R30^\circ$  vacancy arrays, corresponding to oxygen coverages of 1/3 and 1 ML, respectively. We found that these species were energetically *unfavorable* compared to the commensurate oxide-like structures described above. If, however, we assume that Ag vacancies exist, i.e., neglecting the energy cost to create the vacancy, then the *binding energy* is the most favorable of all for coverage 1 ML. We can estimate the concentration of such Ag vacancies using our calculated values of the vacancy formation energy, together with an Arrhenius type equation: For a  $(\sqrt{3} \times \sqrt{3})R30^\circ$  vacancy array with a vacancy concentration of 1/3 ML, the formation energy is 0.53 eV; it is 0.44 eV for a concentration of 0.25 ML, and 0.55 eV for a concentration of 0.11 ML. Considering a temperature of 550 K, corresponding to that around which epoxidation of ethylene takes place, this implies a concentration of thermally induced surface vacancies of less than about  $10^{-5} - 10^{-4}$  ML, which is very small. Furthermore, calculation of the *free energy* shows that this species is less stable than the others. Our results thus do not support the molecular ozone-like species as playing an important role, but point to oxygen atoms of the thin  $(4 \times 4)$  surface-oxide as being the main species actuating epoxidation of ethylene.

### D. Thick oxide formation at Ag(111)

As seen from Fig. 7, our calculations predict that thick oxide-like films can form at Ag(111), but only for low temperatures [e.g.,  $\leq 350$  K (460 K incl. corrections) at atmospheric pressure]. The extremely low sticking coefficient of O<sub>2</sub> at Ag(111),<sup>14</sup> as well as the found low thermal stability of these structures, may hinder their formation. For example, at high temperatures at which diffusion of O (or Ag) atoms can effectively occur, the material may become unstable. Furthermore, when using NO<sub>2</sub> to deliver O atoms to the surface, the substrate has to be held at temperatures *higher* than the temperature at which di-silver oxide decomposes, in order to desorb the NO molecules. Using, however, low temperatures and *atomic oxygen* or ozone (which readily dissociates at the surface) instead of O<sub>2</sub> (or NO<sub>2</sub>), we predict that thick oxide structures could be observed experimentally – providing that diffusion barriers can be overcome.

Interestingly, it was found that di-silver oxide (Ag<sub>2</sub>O) can be prepared using a mixture of ozone and O<sub>2</sub> or microwave generated atomic oxygen, at room temperature on *polycrystalline* silver foil.<sup>65,66,67,68</sup> The oxygen generated in these processes is quite active, for example, small amounts of ozone (5 mol.% O<sub>3</sub> in O<sub>2</sub>) can generate the O partial pressure equivalent to that of a pure O<sub>2</sub> atmosphere at 10<sup>+12</sup> atm. at a temperature of 465 K.<sup>66</sup> Actually, in these mixtures of reaction gas, Ag<sub>2</sub>O can be stable to temperatures in excess of 773 K.<sup>68</sup> In the studies of Waterhouse *et. al.*,<sup>67</sup> it has been found that at room temperature, oxidation of polycrystalline silver foil is improved significantly after the sample has been “scratched”, which generates a high concentration of defects which act as the sites for the oxide film nucleation, highlighting the importance of defects. Also diffusion of oxygen and silver atoms is seemingly improved significantly due to the non-uniformity of the growth.

We note that subsequent to completion of our studies, very recent experimental work reported thick oxide formation at Ag(111) by using a flux of atomic oxygen,<sup>69</sup> thus supporting our findings.

## VII. CONCLUSION

Through density-functional theory calculations, and incorporating the effect of the atmospheric environment, we obtained the pressure-temperature phase diagram for the oxygen/Ag(111) system, which reveals important insights into this system and its function as an oxidation catalyst: The calculations predict that a thin surface-oxide structure is most stable in the temperature and pressure range of ethylene epoxidation and we propose it (and possibly other similar structures) contains the main O species actuating the catalysis. Low coverages of chemisorbed O become more stable for higher temperatures and could also play a role in other oxidation reactions. The only species stable for temperatures in excess

of 720 K (incl. corrections: 830 K), are O atoms adsorbed at under-coordinated surface Ag atoms. Thick bulk-like di-silver oxide can safely be ruled out as playing an important role in the technical catalytic reactions due to the low thermal stability, causing decomposition at temperatures lower than those used in the reactors. They are, however, the most stable structures for strongly O-rich conditions and low temperatures (e.g., up to 330-460 K at atmospheric pressure). Interestingly, the electronic structure of thick oxide surfaces are very similar to that of the thin ( $4 \times 4$ ) surface oxide structure, which raises the question of whether di-silver oxide might be used as a *low-temperature* oxidation catalyst.

A molecular ozone-like species adsorbed at a surface vacancy, as had been proposed in the literature as being the active species for the epoxidation of ethylene, is energetically unfavorable, as is bulk-dissolved oxygen, which strongly questions the latter's hitherto thought crucial role in, e.g., the partial oxidation of methanol to formaldehyde.

We also studied the bulk and (111) surface properties of  $\text{Ag}_2\text{O}$ , the most stable silver oxide. The interaction of oxygen and silver is via a weak hybridization between Ag- $4d-5s$  and O- $2p$  orbitals, with substantial occupation of antibonding orbitals, which explains its low stability. Various terminations of the  $\text{Ag}_2\text{O}(111)$  surface were investigated as a function of the oxygen chemical potential and it is found that the surface with oxygen in the hollow site (i.e., the stoichiometric surface) is most favorable for all of the range of the O chemical potential

considered, while the Ag-terminated surface and surfaces with additional oxygen adsorbed on top of exposed "cus" surface Ag atoms are unfavorable. On investigating the energetics of a transition from commensurate oxide-like structures to the "real" (unstrained) oxide, we find that the transition becomes favorable only at nine O-Ag-O trilayers, which corresponds to  $\sim 4.5$  ML oxygen.

The approach of "*ab initio* atomistic thermodynamics", i.e., of calculating free energies for many possible atomic geometries and predicting the lowest energy structures in contact with species in a gas-phase environment, is a promising approach to investigate a system under different pressure and temperature conditions, in particular, from those of typical theoretical surface science, right up to those of technical heterogeneous catalysis. The obtained phase diagram also shows that if one stays within the region of one phase or along a phase boundary, then a bridging of the pressure gap should be possible. Furthermore, it may be expected that the regions which lie close to the boundaries in the computed surface phase diagram may exhibit enhanced thermal fluctuations, i.e., here the dynamics of atomistic processes may be particularly strong, and this may be particularly relevant for catalysis under realistic conditions. Furthermore, we note however, that an understanding of a *full catalytic cycle*, requires a kinetic modeling that includes all reactant species and intermediates, which for complex systems such as those discussed in the present paper, is not yet possible.

- 
- <sup>1</sup> *Handbook on Heterogeneous Catalysis*, Eds. G. Ertl, H. Knözinger and J. Weitkamp, (Wiley, New York, 1997) Vol.1.
- <sup>2</sup> C. Stampfl, M. V. Ganduglia-Pirovano, K. Reuter, M. Scheffler, *Surf. Sci.* **500**, 368 (2002).
- <sup>3</sup> C. H. F. Peden, in *Surface Science of Catalysis: In situ probes and reaction kinetics*, Eds. D. J. Dwyer and F. M. Hoffmann, American Chemical Society, Washington DC (1992).
- <sup>4</sup> G. A. Somorjai, M. M. Bhasin, J. B. Moffat, and K. I. Tanaka, *Top. Catal.* **19**, 143 (2002).
- <sup>5</sup> K. B. Rider, K. S. Hwang, M. Salmeron, G. A. Somorjai, *J. Amer. Chem. Soc.* **124**, 5588 (2002).
- <sup>6</sup> H. J. Freund, *Surf. Sci.* **500**, 271 (2002).
- <sup>7</sup> K. F. Peters, C. J. Walker, P. Steadman, O. Robach, H. Isern, and S. Ferrer, *Phys. Rev. Lett.* **86**, 5325 (2001).
- <sup>8</sup> B. L. M. Hendriksen and J. W. M. Frenken, *Phys. Rev. Lett.* **89**, 046101 (2002).
- <sup>9</sup> R. A. van Santen and H. P. C. E. Kuipers, *Adv. Catal.* **35**, 265 (1987).
- <sup>10</sup> M. Rocca, L. Vattuone, L. Savio, F. Buatier de Mongeot, U. Valbusa, G. Comelli, S. Lizzit, A. Baraldi, G. Paolucci, J. A. Groeneveld, and E. J. Baerends, *Phys. Rev. B* **63**, 081404(R) (2001).
- <sup>11</sup> L. Savio, L. Vattuone, M. Rocca, F. Buatier de Mongeot, G. Comelli, A. Baraldi, S. Lizzit, and G. Paolucci, *Surf. Sci.* **506**, 213 (2002).
- <sup>12</sup> A. Nagy, G. Mestl, D. Herein, G. Weinberg, E. Kitzelmann, R. Schlögl, *J. Catal.* **182**, 417(1999); A. Nagy, G. Mestl, and R. Schlögl, *J. Catal.* **188**, 58(1999); A. Nagy, and G. Mestl, *Appl. Catal. A* **188**, 337 (1999).
- <sup>13</sup> C. Rehren, M. Muhler, X. Bao, R. Schlögl, and G. Ertl, *Z. Phys. Chem.* **174**, 11 (1991); X. Bao, M. Muhler, B. Pettinger, R. Schlögl, and G. Ertl, *Catal. Lett.* **22**, 215 (1993); H. Schubert, U. Tegtmeier, and R. Schlögl, *Catal. Lett.* **28**, 383 (1994).
- <sup>14</sup> R. B. Grant and R. M. Lambert, *J. Catal.* **92**, 364 (1985); *Surf. Sci.* **146**, 256 (1984).
- <sup>15</sup> R. A. van Santen and C. P. M. de Groot, *J. Catal.* **98**, 530 (1986).
- <sup>16</sup> V. I. Bukhtiyarov, A. I. Boronin, I. P. Prosvirin, and V. I. Savchenko, *J. Catal.* **150**, 262 (1994); V. I. Bukhtiyarov, and I. P. Prosvirin and R. I. Kvon, *Surf. Sci.* **320**, L47 (1994).
- <sup>17</sup> D. Herein, A. Nagy, H. Schubert, G. Weinberg, E. Kitzelmann, and R. Schlögl, *Z. Phys. Chem.* **197**, S67 (1996).
- <sup>18</sup> V. I. Bukhtiyarov, M. Hävecker, V. V. Kaichev, A. Knop-Gericke, R. W. Mayer and R. Schlögl, *Catal. Lett.*, **74**, 121 (2001).
- <sup>19</sup> V. I. Avdeev and G. M. Zhidomirov, *Surf. Sci.* **492**, 137 (2001).
- <sup>20</sup> G. C. Bond and D. T. Thompson, *Catal. Rev. Sci. Eng.*

- 41, 319 (1999), and references therein.
- 21 Y. Uchida, X. Bao, K. Weiss, and R. Schlögl, *Surf. Sci.* **401**, 469 (1998).
  - 22 J. Chevrier, L. Huang, P. Zeppenfeld, and G. Comsa, *Surf. Sci.* **355**, 1 (1996).
  - 23 Th. Schedel-Niedrig, *Phys. Chem. Chem. Phys.* **2**, 3473 (2000).
  - 24 W. X. Li, C. Stampfl, and M. Scheffler, *Phys. Rev. B* **65**, 075407 (2002).
  - 25 W. X. Li, C. Stampfl, and M. Scheffler, *Phys. Rev. B* **67**, 045408 (2003).
  - 26 W. X. Li, C. Stampfl, and M. Scheffler, submitted to *Phys. Rev. Lett.*
  - 27 C.M. Weinert and M. Scheffler, In: *Defects in Semiconductors*, edited by H.J. von Bardeleben. *Mat. Sci. Forum* **10-12**, 25 (1986).
  - 28 M. Scheffler, In: *Physics of Solid Surfaces - 1987*, edited by J. Koukal. Elsevier, Amsterdam 1988, 115 and M. Scheffler and J. Dabrowski, *Phil. Mag. A* **58**, 107 (1988).
  - 29 E. Kaxiras, Y. Bar-Yam, J. D. Joannopoulos, and K. C. Pandey, *Phys. Rev. B* **35**, 9625 (1987).
  - 30 G.-X. Qian, R. Martin, and D.J. Chadi, *Phys. Rev. B* **38**, 7649 (1988).
  - 31 X. G. Wang, W. Weiss, Sh.K. Shaikhutdinov, M. Ritter, M. Petersen, F. Wagner, R. Schlögl, and M. Scheffler, *Phys. Rev. Lett.* **81**, 1038 (1998).
  - 32 K. Reuter and M. Scheffler, *Phys. Rev. B* **65**, 035406 (2002).
  - 33 M. Bockstedte, A. Kley, J. Neugebauer, and M. Scheffler, *Comput. Phys. Commun.* **107**, 187 (1997).
  - 34 J. P. Perdew, K. Burke, and M. Ernzerhof, *Phys. Rev. Lett.* **77**, 3865 (1996).
  - 35 J. A. White and D. M. Bird, *Phys. Rev. B* **50**, 4954 (1994).
  - 36 M. Fuchs, M. Scheffler, *Comput. Phys. Commun.* **116**, 1 (1999).
  - 37 N. Troullier and J. L. Martins, *Phys. Rev. B* **43**, 1993 (1991).
  - 38 S. L. Cunningham, *Phys. Rev. B* **10**, 4988 (1974).
  - 39 J. Neugebauer and M. Scheffler, *Phys. Rev. B* **46**, 16067 (1992).
  - 40 D. R. Stull and H. Prophet, *JANAF Thermochemical Tables*, 2nd ed., U.S. National Bureau of Standards, Washington, D.C. (1971).
  - 41 *CRC Handbook of Chemistry and Physics*, edited by R. C. Weast, 55 ed. Cleveland, Ohio, 1974-1975.
  - 42 M. Scheffler and C. Stampfl, in: *Handbook of Surface Science*, Vol. 2: *Electronic Structure*, (Eds.) K. Horn, M. Scheffler. Elsevier, Amsterdam 1999, *Theory of adsorption on metal substrates*.
  - 43 R. W. G. Wyckoff, *Crystal Structures*, Wiley, New York, 1964.
  - 44 A. F. Wells, *Structural Inorganic Chemistry*, p.1120, 5th edn., Clarendon, Oxford, 1984.
  - 45 L. H. Tjeng, M. B. J. Meinders, J. van Elp, J. Ghijsen, G. A. Sawatzky, and R. L. Johnson, *Phys. Rev. B* **41**, 3190 (1990).
  - 46 M. T. Czyzyk, R. A. de Groot, G. Dalba, P. Fornasini, A. Kisiel, F. Rocca, and E. Burattini, *Phys. Rev. B.* **39**, 9831 (1989).
  - 47 A. Deb and A. K. Chatterjee, *J. Phys: Condens. Matter* **10**, 11719 (1998).
  - 48 M. Staedele M. Moukara, J. A. Majewski, P. Vogl, and A. Görling, *Phys. Rev. B* **59**, 10031 (1999).
  - 49 C. Stampfl and C. G. Van de Walle, *Phys. Rev. B* **59**, 5521 (1999); C. Stampfl, C. G. Van de Walle, D. Vogel, P. Kruger, and J. Pollmann, *Phys. Rev. B* **61**, 7846(R) (2000).
  - 50 C. Stampfl, R. Asahi, and A. J. Freeman, *Phys. Rev. B* **65**, 161204(R) (2002).
  - 51 C. Stampfl (unpublished); R. Asahi, W. Mannstadt, and A. J. Freeman, *Phys. Rev. B* **62**, 2552 (2000).
  - 52 C. I. Carlisle, D. A. King, M. L. Bocquet, J. Cerdá, and P. Sautet, *Phys. Rev. Lett.* **84**, 3899 (2000).
  - 53 J. K. Nørskov, T. Bligaard, A. Logadottir, S. Bahn, L. B. Hansen, M. Bollinger, and H. Bengaard, and references therein, *J. Catal. Priority Comm.* accepted.
  - 54 C. Stampfl and M. Scheffler, *Phys. Rev. B* **54**, 2868 (1996).
  - 55 K. Reuter, M. V. Ganduglia-Pirovano, C. Stampfl, and M. Scheffler, *Phys. Rev. B* **65**, 165403 (2002); *Chem. Phys. Lett.* **352**, 311 (2002).
  - 56 M. Todorova, W. X. Li, M. V. Ganduglia-Pirovano, C. Stampfl, K. Reuter, and M. Scheffler, *Phys. Rev. Lett.* **89**, 096103 (2002).
  - 57 G. Rovida, F. Pratesi, M. Maglietta, and E. Ferroni, *Surf. Sci.* **43**, 230 (1974).
  - 58 C. T. Campbell, *Surf. Sci.* **157**, 43 (1985).
  - 59 S. Bare, K. Griffiths, W. N. Lennard, and H. T. Tang, *Surf. Sci.* **342**, 185 (1995).
  - 60 C. I. Carlisle, T. Fujimoto, W. S. Sim, and D. A. King, *Surf. Sci.* **470**, 15 (2000).
  - 61 B. Pettinger, X. Bao, I. C. Wilcock, M. Muhler, and G. Ertl *Phys. Rev. Lett.* **72**, 1561 (1994); *Angewandte Chemie-Intern. Edition in English* **33**, 85 (1994).
  - 62 Q. Sun, K. Reuter, and M. Scheffler, *Phys. Rev. B*, submitted.
  - 63 T. Zambelli, J. Wintterlin, J. Trost and G. Ertl, *Science* **273**, 1688 (1996); S. Dahl, A. Logadottir, R. C. Egeberg, J. H. Larsen, I. Chorkendorf, E. Törnqvist, and J. K. Nørskov, *Phys. Rev. Lett.* **83**, 1814 (1999); B. Hammer, *Phys. Rev. Lett.* **83**, 3681 (1999).
  - 64 R. Schaub, P. Thostrup, N. Lopez, J. K. Nørskov, E. Lægsgaard, I. Stensgaard, and F. Besenbacher *Phys. Rev. Lett.* **87**, 266104 (2001).
  - 65 M. K. Bhan, P. K. Nag, G. P. Miller, and J. C. Gregory, *J. Vac. Sci. Technol. A* **12**, 699 (1994).
  - 66 K. P. Jayadevan, N. V. Kumar, R. M. Mallya, and K. T. Jacob, *J. Mater. Sci.* **35**, 2429 (2000).
  - 67 G. I. N. Waterhouse, G. A. Bowmaker, and J. B. Metson, *Appl. Surf. Sci.* **183**, 191 (2001).
  - 68 G. I. N. Waterhouse, G. A. Bownmaker and J. B. Metson, *Surf. Interface Anal.* **33**, 401 (2002).
  - 69 Long Li and Judith C. Yang, presented at the MRS Fall meeting, 2002.